IEEE Access
Multidisciplinary | Rapid Review | Open Access Journal

Received December 30, 2021, accepted January 18, 2022, date of publication January 19, 2022, date of current version February 3, 2022.

Digital Object Identifier 10.1109/ACCESS.2022.3144915

Shaped-Pattern Reflectarray Antennas for mm-Wave Networks Using a Simple Cell Topology

BORJA IMAZ-LUEJE[1], (Student Member, IEEE), ÁLVARO F. VAQUERO[2], (Graduate Student Member, IEEE), DANIEL R. PRADO[1], MARCOS R. PINO[1], AND MANUEL ARREBOLA[1], (Senior Member, IEEE)

[1]Group of Signal Theory and Communications, Department of Electrical Engineering, Universidad de Oviedo, 33203 Gijon, Spain
[2]Group of Applied Electromagnetics, Department of Signals, Systems and Radiocommunications, Universidad Politécnica de Madrid, 28040 Madrid, Spain

Corresponding author: Borja Imaz-Lueje (bimaz@uniovi.es)

This work was supported in part by the Ministerio de Ciencia, Innovación y Universidades under Project TEC2017-86619-R and Project IJC2018-035696-I; in part by the Ministerio de Ciencia e Innovación and Agencia Española de Investigación under Project PID2020-114172RB-C21 / AEI / 10.13039/501100011033; in part by the Ministerio de Educación y Formación Profesional under Grant FPU18/02575; and in part by the Vicerrectorado de Investigación of Universidad de Oviedo under Plan de Apoyo y Promoción de la Investigación under Project PAPI-20-PF-15.

ABSTRACT In this paper, it is proposed the use of ultra-thin reflectarrays in some emerging scenarios in the new mm-wave cellular networks such as 5G, Beyond-5G (B5G), and future 6G. To that purpose, two dual-linear polarization reflectarrays are developed to provide coverages in different scenarios at the mm-waves band. Working at 28 GHz, reflectarray designs adapt the radiated field to the coverage area specified in each scenario, through an ultra-thin surface composed of simple cells. To evaluate the antenna performance, two reflectarray prototypes identical in size are manufactured and tested achieving a good trade-off between the performance and the low-cost, low losses and, low-profile characteristics of the antenna. This work demonstrates the good performance of simple topology reflectarrays, being an interesting antenna candidate in the upcoming wireless networks.

INDEX TERMS Reflectarray, dual-polarization, pattern shaping, millimeter wave, 5G new radio, beyond-5G, 6G.

I. INTRODUCTION

The future mobile generations are expected to merge a wide variety of communications systems, offering a considerable improvement in performance in comparison with previous generations. In order to fulfill the current demands of society, the 5th mobile generation (5G) aims to provide high data rates, low latency, and a high connection density [1]. Taking into account how these Key Performance Indicators (KPIs) will be affected in the future, the research community has started to focus on the development of new cellular networks as a solution in Beyond-5G or the next generation, 6G [2].

Within the 5G standard, 3GPP proposed a new radio access technology, called 5G New Radio (5G NR) [3], [4], where it is considered the use of the frequency range between 24250 MHz and 52600 MHz called FR2 or mm-wave band. This relatively idle spectrum has a vast amount of available bandwidth, and it can host services that require high data speeds and low latency in small areas with a dense demand (e.g., cities, offices, public areas, etc.). Therefore, it is expected that mm-wave frequencies will also be exploited by future cellular networks such as B5G or 6G to cope with new services [5]. As a counterpart, the main challenges to be faced in this band are the intrinsic higher path losses and the increasing complexity in system design and manufacturing [6]. In addition, mm-wave signals suffer strong attenuation when interacting with elements of the environment, causing shadowing. The new requirements to be met in mm-wave systems also represent an important issue in the design of the antennas that compose them. Antenna systems must compensate for the higher path loss, generating high gain patterns [7] adjusted to the orography of each scenario.

In this context, several solutions are proposed in the literature. For these new cellular networks, it is proposed the use of antennas with narrow beams and reconfiguration

The associate editor coordinating the review of this manuscript and approving it for publication was Qi Luo.

This work is licensed under a Creative Commons Attribution 4.0 License. For more information, see https://creativecommons.org/licenses/by/4.0/

capabilities [8]. The use of antennas that provide a constant power flux over a certain area can be an alternative, especially in small cells with a low density of users or devices. Regarding the antenna technology, the widespread use of microstrip technology and the harnessing of technologies already used in 4G systems [9], make active microstrip arrays an interesting candidate as an antenna solution. In particular, phased arrays are able to generate narrow multi-beams [10], beam scanning [11], [12], and shaped patterns [13]. However, this type of antenna requires significant improvements to achieve the performance goals in mm-wave frequency band. Improvements that translate into a more complex supply network, a reduction of their energy efficiency, and an increase in the cost. Passive antennas can reduce the complexity and the cost of the design. In this sense, passive arrays can generate high gain beams reducing the complexity in the network supply [14]. However, they are antennas with high losses in their feeding network at mm-waves. Another candidate is the lens antenna which can offer low losses by not requiring a power supply network. In addition, it is a wideband solution to generate beam-steering patterns [15] or constant power flux footprints [16]. However, lens antennas are bulky and heavy. Leaky-Wave Antennas (LWA) are another low-cost alternative which provide high gain, wideband and beam steering patterns [17]. However, the beam generated by an LWA suffers a change in its pointing angle with frequency and significant scanning losses when the beam is away from boresight [18]. Apart from the above-mentioned types, Spatial Feed Arrays (SFA) are a low-cost and low-profile solution able to generate high gain beams with reconfigurable capabilities as well as shaped patterns. Within this group, transmitarrays [19], [20] or metasurfaces [21], [22] can be mentioned due to their performances in several applications such as space communications [23], [24].

Another important SFA antenna is the reflectarray [25]. Compared to phased arrays, it can provide higher aperture efficiencies thanks to their lower losses [26]. Printed reflectarrays can also generate high gain beam-steering and multi-beam patterns [27], [28]. Some works demonstrate the ability of reflectarrays to generate shaped beams and radiated fields over a region in the near field of the antenna. In [29] it is proposed a multilayer reflectarray that generates a shaped pattern for a Local Multipoint Distribution System (LMDS). In [30], it is proposed a reflectarray for a 5G application to produce a field close to the antenna with amplitude and phase constraints. Nevertheless, printed reflectarrays have an inherent narrow bandwidth [31] but it is not a problem in mm-wave cellular networks when working in relatively small frequency slots (∼400 MHz) [4].

In this work, it is proposed the use of reflectarray antennas in two potential cellular scenarios working in mm-wave band. In the first scenario, the aim is to provide a near field coverage area in an indoor environment, while in the second the goal is to generate a far field for mobile cells in an outdoor environment. For this purpose, two low-cost, ultra-thin reflectarray antennas with identical optics and formed by a single layer of rectangular patches have been designed. The generalized Intersection Approach (gIA) [32], [35] is used to seek the phases that each element must introduce in the incident field to meet the radiated field requirements marked in each scenario including the phase shift limitations derived from the use of a simple cell. With these phases and knowing the radiant element electromagnetic response, a reflectarray layout is obtained using Method of Moments based on Local Periodicity (MoM-LP) [35]. The performance of each design is assessed through a simulation based on MoM-LP and the manufacture and measurement of a prototype. Besides, the prototype performances are compared to published reflectarray solutions.

II. DEFINITION OF SCENARIOS AND REQUIREMENTS

As discussed before, the high path losses suffered by mm-wave signals and their exponential dependence with the link distance, lead to work with architectures where their elements (base stations, UE – User Equipment, etc.) are close together. Furthermore, the penetration losses dramatically increase in mm-waves, making the coverage inside buildings from outdoor base stations a challenge. This promotes the deployment of specific cellular networks for indoor and outdoor environments with a small radius.

In indoor scenarios, the use of low-cost, low-power femtocells are proposed as architecture. Their base stations offer many benefits such as better coverage or the increase of channel capacity, among others [36]. To avoid NLOS communications, femtocells seek to provide coverage shaped according to the physical elements which are in the indoor environment (e.g., corridors, compartments in offices, halls . . .). Regarding outdoor scenarios, it is proposed the use of a central base station and a set of small cells placed within the footprint coverage to increase the data rates in some specific areas [37]. As it happens in the indoor case, the use of shaped patterns in this type of cell provides flexibility to generate coverage according to the orography of the scenario.

In this paper, two reflectarray antennas are designed: one for an indoor scenario (Indoor Reflectarray Antenna – IRA) and the other for an outdoor scenario (Outdoor Reflectarray Antenna – ORA). Both designs must work in dual-linear polarization (V- and H-polarization according to Fig. 1) in Ka-band at 28 GHz (frequency that belongs to the mm-wave band). Vertical (V) and horizontal (H) axes correspond to the X and Y axes defined in the reflectarray coordinate system of Fig. 2. The requirements that must fulfill the field in each design are detailed in the following sections.

A. INDOOR SCENARIO

(see Fig. 1(a)), the aim is to design a reflectarray for use it in a femtocell base station, which generates a coverage on a conventional office desktop of dimensions 1.2×0.4 m^2 and a height of 1.0 m. The reflectarray is placed on a wall near the desk 2.1 m above the floor, while the feed will be placed on the ceiling. The distance between reflectarray and the desktop will be 1.9 m. On the desktop surface, the reflectarray must

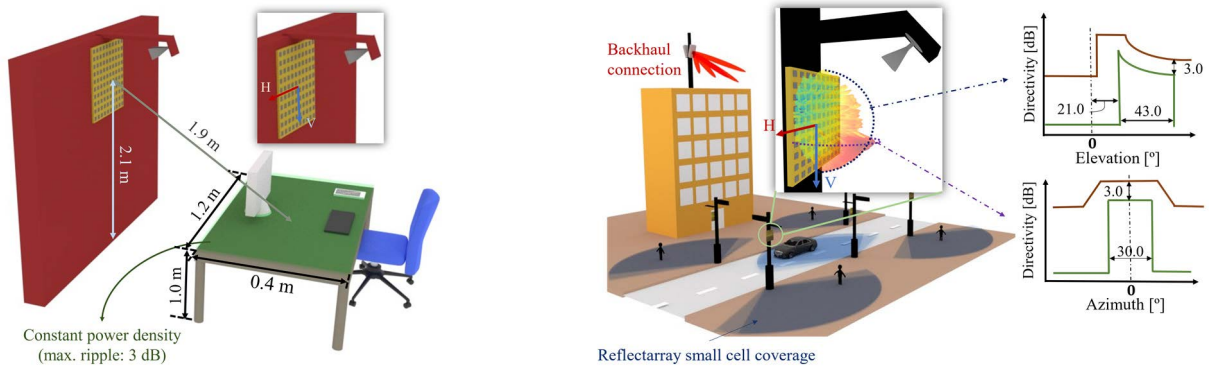

FIGURE 1. Proposed 5G scenarios and antenna requirements: (a) Reflectarray to give coverage to an office desktop (green surface) for base station femtocell. Within the femtocell, the radiated power density must be uniform with a maximum ripple of 3 dB; (b) Reflectarray for small cell base station to provide communication to the user. The antenna must generate a sectored radiation pattern in azimuth and a squared cosecant pattern in elevation (blue). The characteristics of this pattern in its main cuts are shown in the right plots.

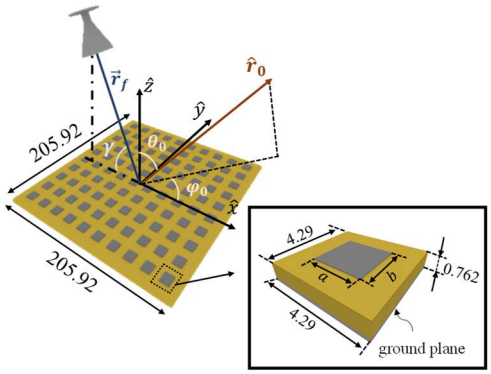

FIGURE 2. Sketch of the reflectarray structure and cell characteristics for both designs. The reflectarray is rectangular and is formed by variable patches on diClad 880 (dark yellow) substrate backed by a ground plane. The feed is placed in the XZ plane with regard to the reflectarray coordinate system. All dimensions are in mm.

generate a smooth field amplitude, with a maximum ripple of 3 dB. Outside this area, the field amplitude must decrease at levels 12 dB lower than the average values in the coverage area. The backhaul of the base station may be implemented with wired technology such as optic fiber.

B. OUTDOOR SCENARIO

Regarding the outdoor scenario (see Fig. 1(b)), a reflectarray antenna is designed to be used in small cell base stations distributed in a street to provide end-user coverage. The reflectarray antennas, installed on the lampposts along the street, must generate a sectorial coverage in azimuth and a squared cosecant beam in elevation. The width of this area will be 43.0° in elevation and 30.0° in azimuth. To avoid blockage by the feed, a tilt of 21.0° in elevation is introduced. A ripple of 3 dB is allowed in the coverage area, while the field level outside it must at least 12 dB lower. The backhaul communication between the small cells and central base station may be implemented using an independent radio link.

III. REFLECTARRAY ANTENNA DEFINITION

A. ANTENNA OPTICS AND UNIT CELL

The two reflectarray antennas are identical in size and shape with different layouts. As shown in Fig. 2, the common structure consists of a single-offset configuration where the reflectarray panel is formed by 1936 elements distributed in a squared grid of 44 × 44 elements. The periodicity is 4.29 mm ($0.4\lambda_0$ at 28 GHz) in both axes, which avoids grating lobes [25]. To facilitate the assembly with the supporting structure, a dielectric frame of 8.58 mm ($0.8\lambda_0$) is left at the edges [32]. Thus, the total size of the panel is 205.92 mm × 205.92 mm.

The feed selected is the Narda 665-20 horn antenna of 18.6 dBi gain at the working frequency. Its phase center at 28 GHz is placed at coordinates (−79.30,0.00,200.20) mm regarding the reflectarray coordinate system (see Fig. 2). The feed has an illumination angle (γ) of 20.0°, which generates an average taper on the reflectarray surface of −15.8 dB for V-polarization and −15.7 dB for H-polarization. The antenna optics has an f/D ratio of 0.97.

The reflectarray element is a single rectangular patch backed by a ground plane. DiClad 880 ($\varepsilon_r = 2.3, \tan\delta = 0.005$) is selected as substrate, with a thickness of 0.762 mm. Fig. 3 (a) shows the direct reflection coefficient ρ_{XX} at 28 GHz for different angles of incidence. Fig. 3 (b) shows the response of ρ_{XX} at different frequencies considering an oblique incidence of $(\theta, \varphi) = (40°, 45°)$. A small phase variation is observed under oblique conditions, which demonstrates the angular robustness of this unit cell topology. The coefficient ρ_{YY} presents a similar behavior to ρ_{XX}.

Regarding the magnitude, the cell losses are also stable and low for different frequencies and angles of incidence. The maximum losses are less than 0.5 dB, and they occur at 30.0 GHz with an incidence of $(\theta, \varphi) = (40°, 45°)$. In all cases, the cell structure can provide a maximum phase-shift of 260°. This phase-shift range does not cover an entire phase cycle (360°) and the design technique will be adapted to consider this. Despite having a limited phase-shift range,

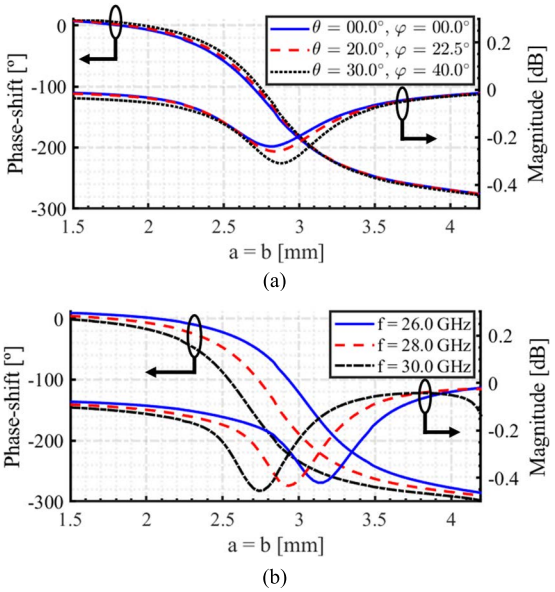

FIGURE 3. Response of the direct reflection coefficient ρ_{XX} in phase (right) and magnitude (left) as a function of the patch dimensions (a, b) for: (a) different angles of incidence at 28 GHz; (b) different frequencies considering $(\theta, \varphi) = (40.0°, 45.0°)$.

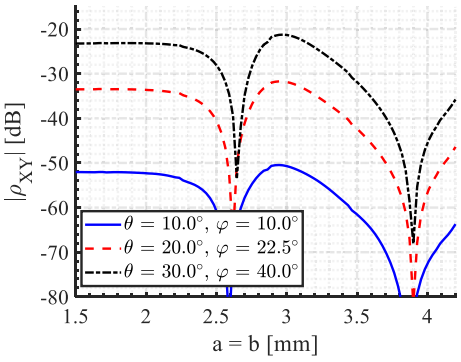

FIGURE 4. Magnitude of the cross-coefficient ρ_{XY} for different angles of incidence at 28 GHz.

the topology allows the design of a low-profile and low-cost antenna, which is interesting for the application at hand. Fig. 4 shows the magnitude of the cross-coefficient ρ_{XY} for different angles of incidence at the design frequency. A low crosspolar level and a high isolation between both polarizations are ensured due to low magnitude of cross-coefficients, which are lower than -20 dB. A similar response is found for the cross-coefficient ρ_{YX}.

B. DESIGN PROCEDURE

The process followed to design both reflectarray antennas is depicted in Fig. 5. The generalized Intersection Approach (gIA) is used to obtain a radiated field adjusted to certain specifications, either far- or near-field. The gIA iteratively searches for the intersection between two sets (see Fig. 6): the set of fields that are radiated by the antenna ($\mathcal{R}$), and the set of fields that satisfy the requirements ($\mathcal{M}$) [33]. The search is based on the Alternate Projection method and performs the

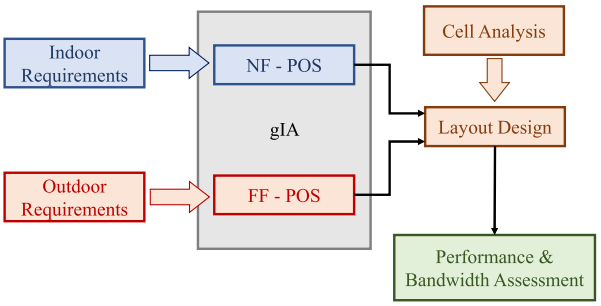

FIGURE 5. Flowchart of reflectarrays design procedure.

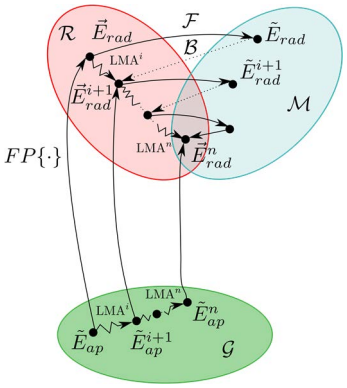

FIGURE 6. Schematic representation of the generalized intersection approach (gIA).

following operations:

$$\vec{E}_{rad}^{\,i+1} = \mathcal{B}[\mathcal{F}\left(\vec{E}_{rad}^{\,i}\right)] \tag{1}$$

where $\vec{E}_{rad}$ is the field radiated by the antenna, either near- or far-field; $\mathcal{F}$ is the forward projector and $\mathcal{B}$ is the backward projector.

The forward projector $\mathcal{F}$ projects a radiated field by the antenna (i.e., it belongs to $\mathcal{R}$) onto a field that satisfies the specifications (i.e., it belongs to $\mathcal{M}$). Then, the backward projector retrieves a field of $\mathcal{M}$ onto a point in $\mathcal{R}$. These two operations are performed iteratively to find the intersection between both sets, and, if that is not possible, to minimize the distance between them.

For the implementation of the backward projector, the gIA employs the following strategy. Starting from a field in the aperture ($\tilde{E}_{ap}$, see Fig. 6), a forward propagation (FP) is applied to obtain a radiated field, either near- or far-field, $\tilde{E}_{rad}$. Then, the forward projector projects it onto a field within the specifications ($\tilde{E}_{rad}$). In this case, the forward projector is defined to satisfy

$$\mathrm{T_{low}} \leq \left|\tilde{E}_{rad}\right| \leq \mathrm{T_{upper}} \tag{2}$$

where $\tilde{E}_{rad}$ is the field within the specifications and belongs to M; and $\mathrm{T_{low}}$ and $\mathrm{T_{upper}}$ are the boundaries of the upper and lower specifications.

The gIA defines a functional d to evaluate the distance from one point in $\mathcal{R}$ to another in $\mathcal{M}$. This functional is defined as

$$\mathrm{d} = \mathrm{dist}\left(|\vec{E}_{rad}|^2, \mathcal{F}\left\{|\vec{E}_{rad}|^2\right\}\right). \tag{3}$$

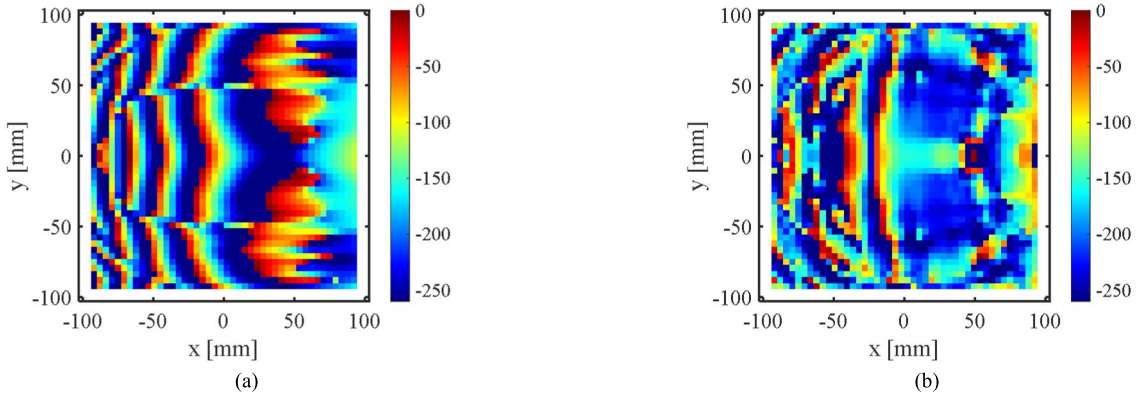

FIGURE 7. Phase distribution of reflection coefficients of each element after a POS for V-polarization: (a) IRA design; (b) ORA design. Phases for H-polarization are similar in both cases.

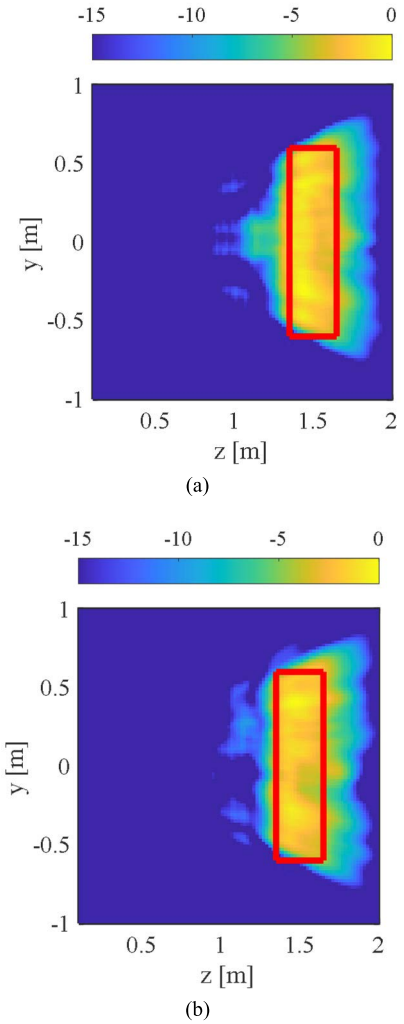

FIGURE 8. IRA design: normalized measured E-Field copolar component in dB at 28 GHz: (a) Vertical polarization; (b) Horizontal polarization. The red rectangle shows the contour of the coverage area.

The Levenberg-Marquardt algorithm (LMA) [38] is used to minimize d in each iteration of the gIA. After several iterations of the gIA, the intersection between both sets may be found, obtaining a field radiated by the antenna that complies with the specifications. If the intersection is not reached, it obtains a radiated field whose distance to $\tilde{E}_{rad}$ is minimal. Since a phase-only synthesis is used, the degree of freedom is the phase-shift distribution of the reflection coefficients on the reflectarray surface. Two independent syntheses are carried out to obtain the reflection coefficients for each polarization. As previously mentioned, the gIA only considers a maximum phase-shift range of 260°. This limitation is included in the implementation of the LMA and it is considered in each iteration of the algorithm, ensuring that the solution is reachable by the selected element.

For the IRA, the constraints are imposed in the amplitude of the radiated near-field [30], while in the ORA are imposed in the far-field [32]. The horn antenna is accurately characterized with the electromagnetic software CST Microwave Studio [40]. The starting point is a phase distribution $\phi\,(x_{\mathrm{m}}, y_{\mathrm{m}})$ that generates a collimate pencil beam in a certain direction (θ_0, φ_0). According to the traditional array theory, this phase distribution is obtained as [25],

$$\phi\,(x_m, y_m) = k_0[d_m - (x_m \cos\varphi_0 + y_m \sin\varphi_0)\sin\theta_0] \quad (4)$$

where k_0 is the propagation constant in vacuum, d_m is the distance from the phase center of the feed to the m-ith element and (x_m, y_m) the position of the m-ith element in the reflectarray coordinate system (see Fig.2). For the IRA, a phase distribution that generates a beam pointing at the center of the coverage area $(\theta_0, \varphi_0) = (35.0°, 0.0°)$ is taken as starting point. In the outdoor case, the gIA starts with a $\phi\,(x_{\mathrm{m}}, y_{\mathrm{m}})$ that generates a beam around the direction of maximum radiation of the cosecant pattern $(\theta_0, \varphi_0) = (20.5°, 0.0°)$. The resulting phases after the POS optimization in V-polarization for both designs are shown in Fig. 7. Although in both cases the starting phase-shift distribution is similar, by working with different requirements the resulting phase distributions are very different. Similar synthetized phases were obtained for H-polarization.

Once the phase distribution has been obtained, the elements of the reflectarray are properly designed to introduce

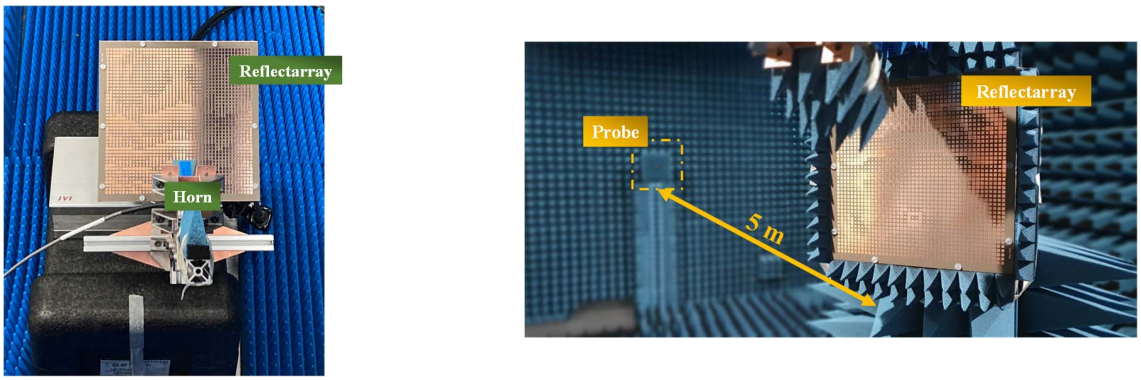

(a) (b)

FIGURE 9. Measurement setups used for the experimental validation of the reflectarray designs at the Universidad de Oviedo facilities: (a) Planar acquisition range for the indoor design and (b) Spherical Compact Range for the Outdoor Scenario.

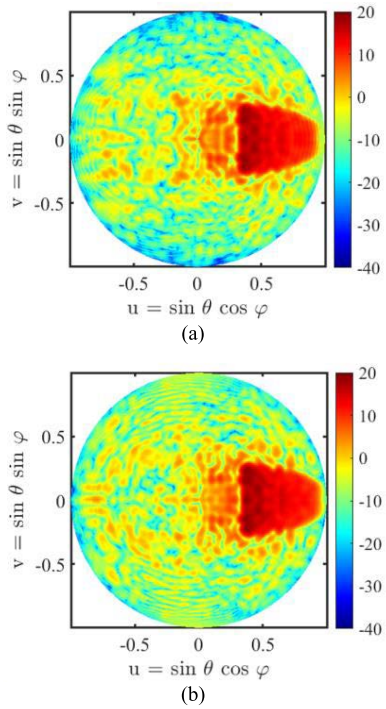

FIGURE 10. ORA design. Copolar far field measured at 28 GHz on a u-v grid: (a) V-polarization; (b) H-polarization. Colorbar corresponds with the directivity in dBi.

the required phase shift. The dimensions a and b of each printed patch (see Fig. 2) are chosen to adjust the phase response of the cell with the phase distribution in both linear polarizations obtained after the synthesis at the same time. This process is carried out element by element, considering a local periodic environment and the real angle of incidence for each cell. Although the proposed cell topology does not provide a total independence between both linear polarizations, a good isolation is ensured between them. Indeed, the design process uses a zero-finding routine that adjusts the patch sizes for both linear polarizations at the same time, taking the polarization coupling that it may exist between them into account [39]. After this process, a layout of 44×44 printed patch elements for each design is obtained.

To assess the antenna performance, the layouts are evaluated through an electromagnetic simulation using a Method of Moments based on Local Periodicity [35] and the field computation used in the optimization process.

IV. EXPERIMENTAL RESULTS

The two designed layouts have been manufactured and measured in the facilities of University of Oviedo. They are placed on an aluminum structure that follows the antenna definition described in Fig. 2.

Although both designs share the structure, the evaluation setup is different. The IRA is measured in the planar acquisition range. The reflectarray structure (see Fig. 9(a)) is tilted $\theta_0 = 35°$ to radiate the coverage parallel to the near field probe aperture (an open-ended Ka-band waveguide). Due to the limitations on the facilities, the electric field is measured in a plane at 500 mm away from the reflectarray. Then, the electric field at the coverage plane is obtained by applying an NF - NF transformation with TICRA software GRASP [41]. Conversely, the ORA has been measured in the spherical range anechoic chamber. The reflectarray is placed 5 m from the probe (a Ka-band pyramidal horn antenna) as shown in Fig. 9(b). Since the probe is in the near-field of the reflectarray, the far field is obtained through an NF-FF transformation using the software SNIFT from TICRA [42].

In the following sub-sections, the performance of both designs is evaluated focusing on the ripple of the coverage zone and the field level outside it. To this purpose, two figures of merit are used: the percentage of compliance and the maximum deviation with the mask requirements. The first figure of merit is calculated as the ratio of the number of field points that satisfy the requirements to the total number of points. The maximum deviation value was the difference between the requirements and the field point furthest away from them. These figures are evaluated in the coverage area and outside it, matching the masks to the field obtained at 28 GHz. As no absolute field or directivity is considered as a requirement, the masks are adjusted to the simulated or measured field in each case.

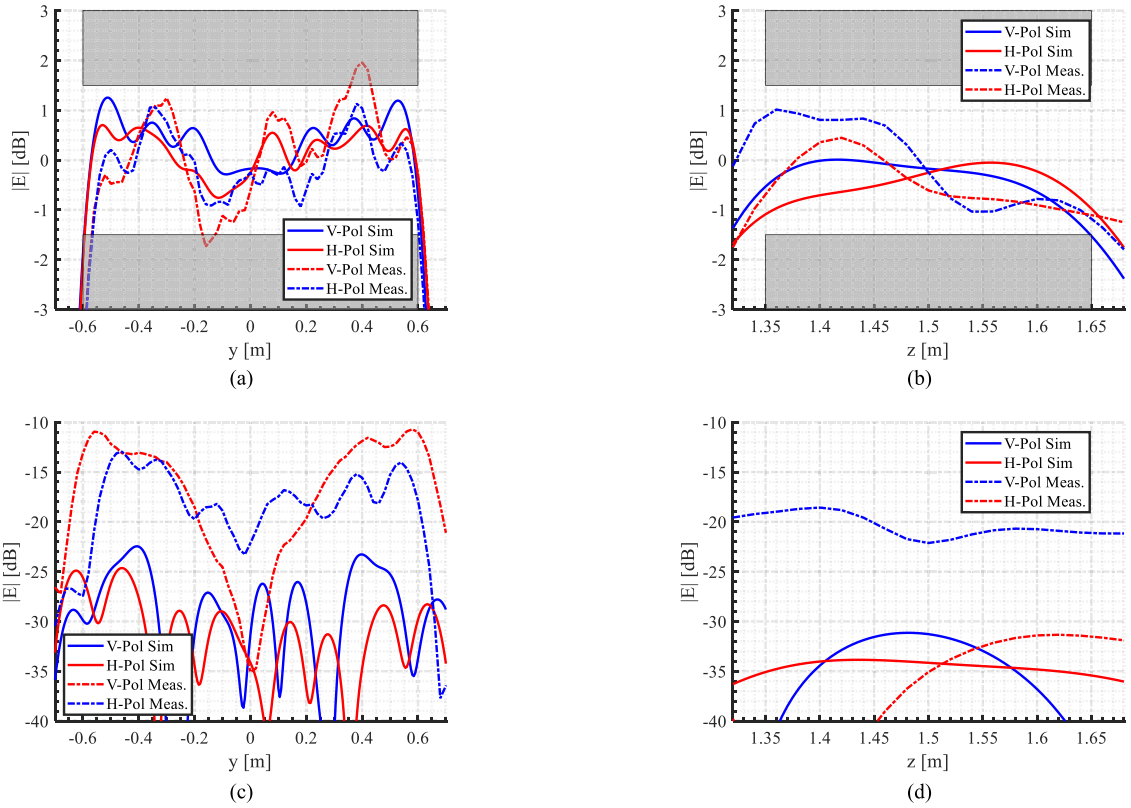

FIGURE 11. Measurement performance of IRA design at 28 GHz. (a,c) Cut $z = 1.5m$ and (b,d) Cut $y = 0.0m$. (a,b) E-Field copolar component and (c,d) E-Field crosspolar component. All fields are normalized to the average of the E-Field copolar component.

A. INDOOR SCENARIO

Figs. 8 and 11 show the achieved coverage in simulation and measured for both polarizations. The simulated field nearly satisfies the requirements with compliance above 99% for both polarizations. Excellent results are also achieved in the measured field where the compliance is above 87% for V- and H-polarizations. The lower compliance is due to a higher ripple (Fig. 11) and the appearance of shadowing areas at the edges of the coverage which also increase the field deviation (see Fig. 8). They are caused by the pattern of the feed horn that produces the incident field, which makes it difficult to generate ideal rectangular contours. According to the obtained compliance figures, these effects do not have a significant impact on the antenna performance.

These results demonstrate that the reflectarray concentrates most of the power within the coverage area, decreasing rapidly the field outside it. In this external area, the simulated and measured field has compliance above 79% for both polarizations. As it can be seen in Fig. 8, a transition zone appears around the coverage area, which limits the degree of compliance in this zone. There is not a standard definition of crosspolar for the near-field. However, to evaluate the level of the non-desired E-Field component, Fig. 11(c,d) show the amplitude of the field for the V-polarization when the reflectarray is illuminated in the H-polarization and vice versa. These results ensure a high isolation between both polarizations. According to this definition, the crosspolar components are notably lower than the copolar one (at least 10 dB lower).

B. OUTDOOR SCENARIO

Fig. 10 shows the far field measured for the ORA design at 28 GHz for both polarizations. It shows how the shaped pattern concentrates most of its power within the coverage area set as a requirement. Fig. 12 shows the main cuts of the patterns shown in Fig. 11. A good agreement between simulation and measurements is achieved. In the coverage area, simulated far field almost fulfills the requirements in the elevation cut and fulfills specifications in the azimuth cut. The compliance is greater than 88 % and the maximum deviation is 1.6 dB in both polarizations. Experimental results also meet to a great extent the requirements, although the ripple increases slightly, causing a maximum deviation up to 2.25 dB. However, the degree of compliance remains at 88 % because the measured field is better adjusted to the masks as the power is distributed more uniformly along the slope of the cosecant.

According to Fig. 12, outside the coverage area, the field simulated and measured rapidly decreases with field values adjusted to the mask. The compliance in this area in both cases and for both polarizations is greater than 99 % with a deviation of 1 dB in simulation and about 2 dB in measurements. The crosspolar level in both polarizations remain 20 dB lower than the copolar in the whole coverage

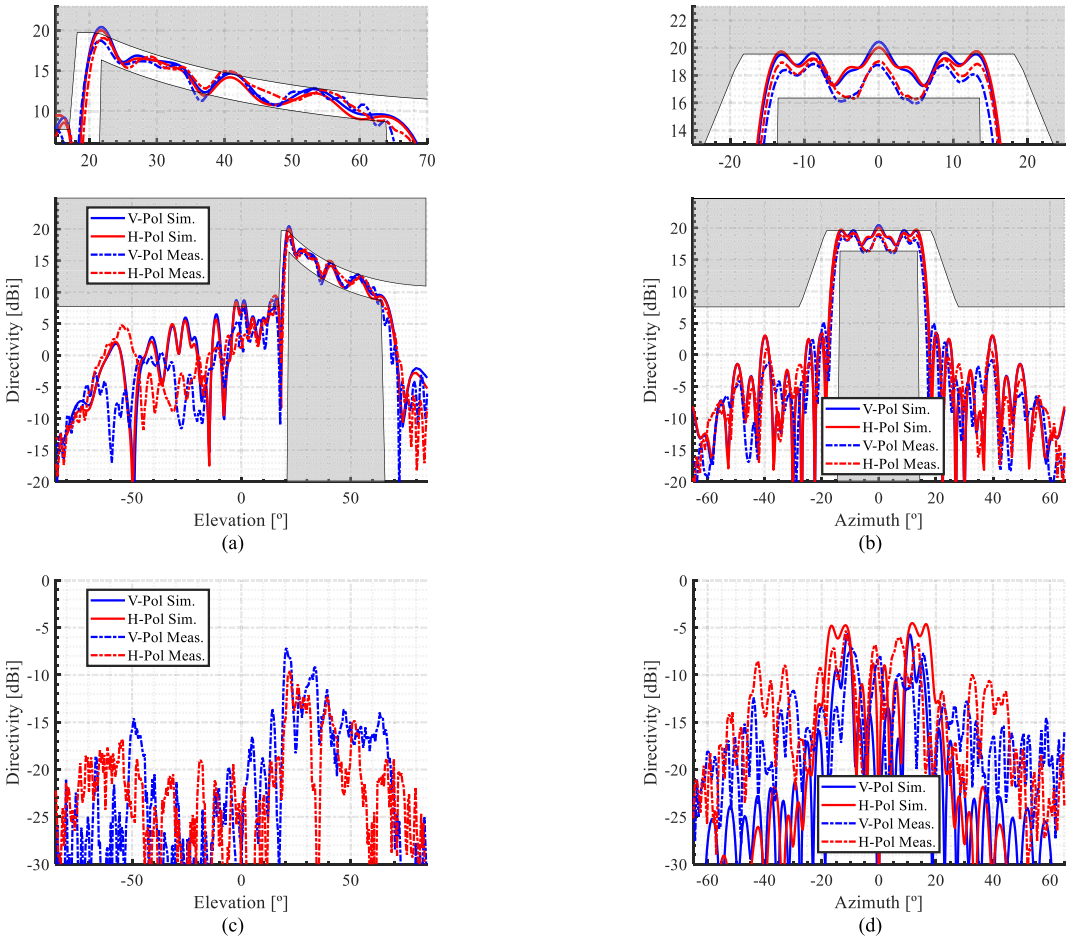

FIGURE 12. ORA design measured performance at 28 GHz. (a,c) Elevation cut and (b,d) Azimuth cut at $\theta_{elev} = 21.0°$. (a,b) Copolar patterns and (c,d) crosspolar patterns.

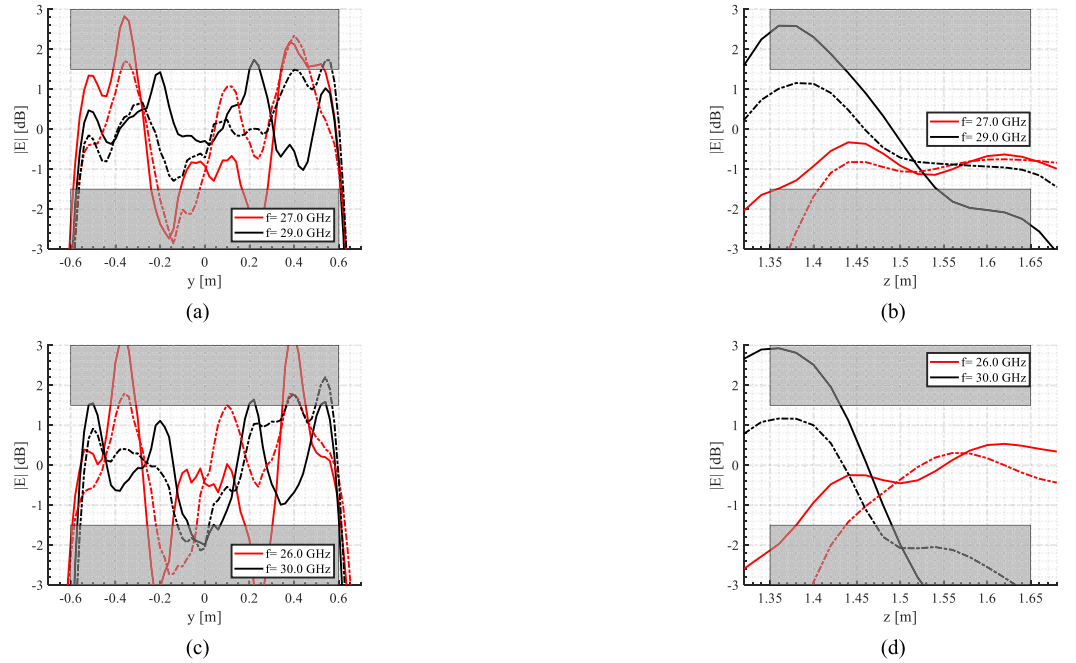

FIGURE 13. IRA measured bandwidth performance. (a,c) Cut $z = 1.5m$and (b,d) Cut $y = 0.0m$. Measurements in (a,b) 2 GHz bandwidth and (c,d) 4 GHz bandwidth. Solid lines correspond with V-polarization and dotted lines with H-polarization.

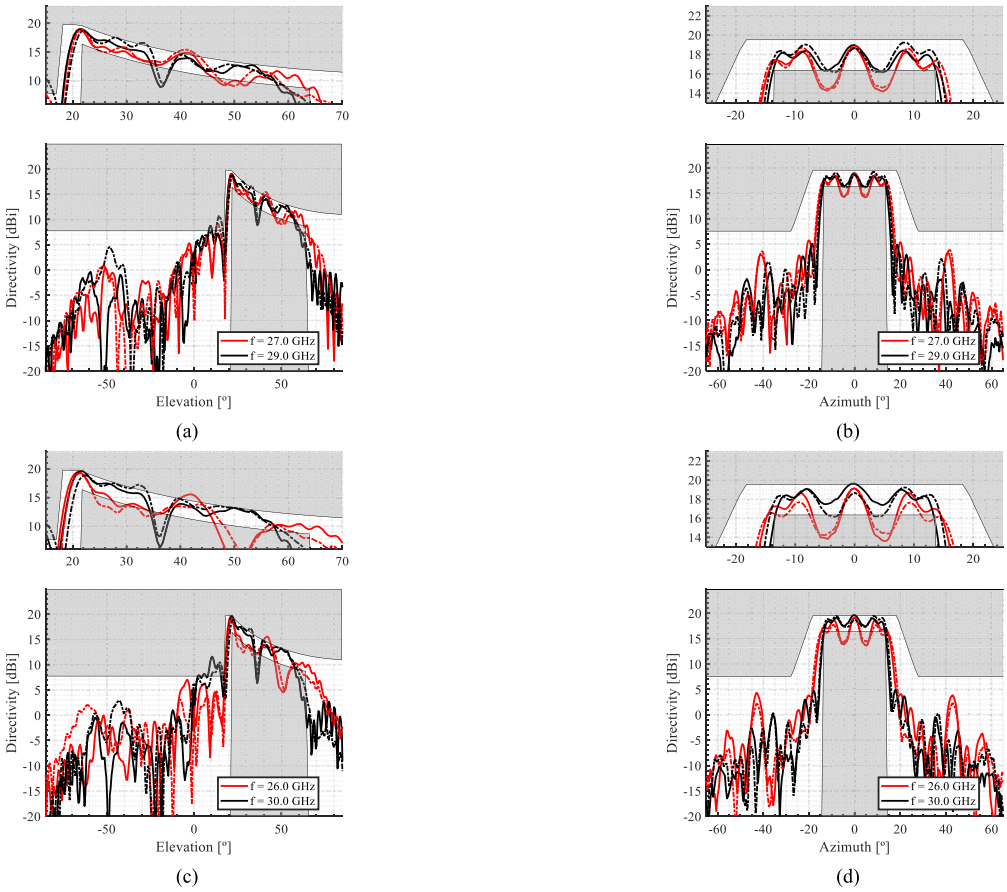

FIGURE 14. ORA measured bandwidth performance. Main cuts in (a,c) Elevation and (b,d) Azimuth. Measurements in (a,b) 2 GHz bandwidth and (c,d) 4 GHz bandwidth. Solid lines correspond with V-polarization and dotted lines with H-polarization.

area. Moreover, this level is 25 dB lower than the copolar in the main cuts. Therefore, the pattern has a good crosspolar discrimination.

C. BANDWIDTH PERFORMANCE

In the following section, the in-band performance of the reflectarray prototypes has been evaluated in a bandwidth of 2 and 4 GHz around the design frequency. Figs. 13 and 14 show the main cuts of the measured field at the extreme frequencies while Table 1 lists the degree of compliance and maximum deviation, for each polarization, design, and field area under study. In this case, the masks of requirements are adjusted to the field measured at 28 GHz.

According to Fig. 13, the field in the IRA prototype remains largely within the requirements between 27 and 29 GHz with an increase of the ripple. This can be also seen in Table 1. The radiated field in both polarizations have a compliance above 67% in 2 GHz of bandwidth. Indeed, H polarization achieves compliance above 70 % in the 4 GHz of bandwidth. Outside the coverage zone, the compliance is above 90 % from 26 to 30 GHz.

The ORA prototype also presents a good in-band performance inside the coverage zone, with compliance above 72 % from 27 to 29 GHz. As shown in Fig. 14(c,d), at extreme frequencies, shadow zones appear with significant drops in the field level. Furthermore, deformations of the coverage area increase the maximum deviation. This, together with a higher ripple, considerably decreases the compliance. Outside the coverage area, the radiated field in both polarizations almost meet the requirements in the frequency range under study, with compliance above 98%.

The higher ripple observed in both designs within the coverage area is due to the use of a cell topology with a limited phase-shift range of 260°. In addition, a POS at central frequency is performed. Therefore, the band response of the antenna has not been considered through the design process. Despite this, in both designs a good trade-off between in-band performance and physical characteristics is demonstrated.

D. COMPARISON WITH OTHER WORKS

Regarding the IRA design and reflectarrays working in the near-field, most works in the literature deal with near-field focusing spots [43]–[45]. This is the first work in the literature that proposes a dual-linear-polarized reflectarray with a non-focusing shaped-beam for near-field coverage.

Regarding the ORA design, many dual-polarized reflectarrays have been proposed in the literature for different far field applications. Considering the application and the frequency

TABLE 1. Evaluation of the performance of reflectarray designs in terms of compliance and maximum deviation from requirements.

f [GHz]	IRA (V - Pol/H - Pol)				ORA (V - Pol/H - Pol)			
	Coverage ripple		Outside level		Coverage ripple		Outside level	
	Max. Dev [dB]	3 dB Comp. [%]	Max. Dev [dB]	12 dB Comp. [%]	Max. Dev [dB]	3 dB Comp. [%]	Max. Dev [dB]	12 dB Comp. [%]
26.00	6.17/5.01	64.2/77.1	14.7/12.7	93.8/94.7	5.37/5.01	56.8/44.4	0.51/1.03	99.9/99.9
27.00	6.85/9.33	67.1/71.2	13.5/12.8	94.7/95.2	3.24/3.18	75.6/72.2	0.92/1.44	99.9/99.9
28.00	11.4/11.5	92.3/87. 3	13.1/13.1	95.2/94.4	2.25/1.09	88.1/93.6	2.00/2.06	99.6/99.7
29.00	12.6/15.8	69.6/85.4	15.2/14.0	94.9/93.3	4.32/2.90	72.1/81.1	2.64/3.06	99.2/99.0
30.00	14.6/28.8	52.7/75.3	16.8/14.6	94.4/92.5	7.78/4.27	66.9/74.3	4.32/4.29	98.0/98.1

TABLE 2. Comparison of different dual-polarized reflectarrays for far-field applications.

Ref.	Cell		RA size [λ_0]	Diagram Pattern	Frequency Band (f_0 GHz)	Bandwidth [$\%f_0$]	Polarization
	Topology	Number of layers					
[29]	Stacked Variable Size Patches	2	15 x 15	El: Cosecant-Squared Az: Sectorial	K (25.5)	8.0	Dual-linear
[46]	Two Slots cut into a metallic plate	1	21 x 13	E-Plane: Pencil beam H-Plane: Cosecant-Squared	X (17.0)	7.0	Dual-linear
[47]	Octagonal patches and rings	1	15 x 15	Pencil beam	Ka (28.0)	13.9	Dual-linear
ORA	Variable Size Patches	1	19 x 19	El: Cosecant-Squared Az: Sectorial	Ka (28.0)	7.0	Dual-linear

band at hand, Table 2 lists some of these works, comparing them to the ORA design. Different parameters are considered in the comparison: cell topology, reflectarray size, diagram pattern, frequency band, bandwidth, and polarization. In [29] a reflectarray to generate a shaped pattern for an outdoor coverage (squared cosecant) is proposed. However, it does not work in the frequency band of interest (Ka band) and uses a more complex cell. In [46] a reflectarray antenna which generates a shaped beam pattern using a single-layer cell topology is presented. In [47] a dual-linear-polarized reflectarray composed of single layer elements is presented. Although the reflectarray works in Ka band, it only generates a pencil beam. Generally, the ORA design generates a coverage area adjusted to the requirements of the application using a simpler cell topology. In addition, the relative bandwidth of the ORA design is similar to other reported designs that generate similar shaped beams such as [29] and [46].

V. CONCLUSION

Two dual-polarized reflectarrays are proposed as antenna solutions for some of the scenarios to be covered with mm-wave technologies. Working in Ka-band at 28 GHz, the reflectarrays are designed to be used as fronthaul base stations in an indoor and outdoor environment, respectively. The proposed antennas are a low-cost and low-profile solution comprised of a single layer of 1936 patches with a size of approximately 200×200 mm^2 and an f/D ratio of the whole antenna closes to one. In the design process, the gIA algorithm is used in a POS at central frequency, to obtain a phase distribution that generates a radiated field adjusted to the coverage specified in each scenario. The algorithm considers the phase restrictions imposed by the simple cell topology.

Knowing the behavior of the unit cell, the phase distributions are translated into layouts. The performance of both designs is evaluated through a MoM-LP simulation and by manufacturing and measuring two prototypes. Good agreement is observed between simulations and measurements in both designs, which practically satisfies the requirements in the coverage area at central frequency. The behavior of the field is degraded in band, increasing the ripple in the coverage area, and generating zones of shadow. This is due to the use of a simple cell with limited phase-shift range and the design is performed considering just the central frequency. Despite this, both designs largely meet the requirements imposed in both scenarios at 28 GHz, presenting a good performance over 2 GHz, a bandwidth equivalent to 5 times the bandwidth normally used in 5G.

This contribution demonstrates the versatility of reflectarrays to work in different scenarios at mm-waves, offering a low-profile, low-loss and low-cost solution with a good antenna performance despite the use of a very simple cell topology with significant phase limitations.

REFERENCES

[1] A. Biswas and V. R. Gupta, "Design aspects of 5G: Frequency allocation, services and MIMO antennas," *Eng. Appl. Sci. Res.*, vol. 47, pp. 103–110, Mar. 2020, doi: 10.14456/easr.2020.10.

[2] M. Latva-Aho and K. Leppänen, "Key drivers and research challengues for 6G ubiquous wireless intelligence," 6G Flagship, Univ. Oulu, Oulu, Finland, Tech. Rep. 6G Research Visions 1, Sep. 2019. [Online]. Available: http://jultika.oulu.fi/files/isbn9789526223544.pdf

[3] "3GPP release 15 description," 3GPP, Tech. Rep. 3GPP TR 21.915 v15.0.0, 2019. [Online]. Available: https://www.3gpp.org/release-15
[4] "3GPP release 16 description," 3GPP, Tech. Rep. 3GPP TR 21.916 v16.0.0, 2020. [Online]. Available: https://www.3gpp.org/release-16
[5] K. Samdanis and T. Taleb, "The road beyond 5G: A vision and insight of the key technologies," *IEEE Netw.*, vol. 34, no. 2, pp. 135–141, Mar./Apr. 2020, doi: 10.1109/MNET.001.1900228.
[6] J. G. Andrews, S. Buzzi, W. Choi, S. V. Hanly, A. Lozano, A. C. K. Soong, and J. C. Zhang, "What will 5G be?" *IEEE J. Sel. Areas Commun.*, vol. 32, no. 6, pp. 1065–1082, Jun. 2014, doi: 10.1109/JSAC.2014.2328098.
[7] R. Dilli, "Analysis of 5G wireless systems in FR1 and FR2 frequency bands," presented at the 2nd Int. Conf. Innov. Mech. Ind. Appl. (ICIMIA), Mar. 2020, doi: 10.1109/ICIMIA48430.2020.9074973.
[8] F. Boccardi, R. W. Heath, Jr., A. Lozano, T. L. Marzetta, and P. Popovski, "Five disruptive technology directions for 5G," *IEEE Commun. Mag.*, vol. 52, no. 2, pp. 74–80, Feb. 2014, doi: 10.1109/MCOM.2014.6736746.
[9] B. Clerck and C. Oestges, "MIMO in LTE, LTE-advance and WiMaX," in *MIMO Wireless Networks*, 2nd ed. Waltham, MA, USA, 2007, ch. 14, p. 597.
[10] H.-T. Chou, "Design methodology for the multi-beam phased array of antennas with relatively arbitrary coverage sector," in *Proc. 11th Eur. Conf. Antennas Propag. (EUCAP)*, Paris, France, Mar. 2017, pp. 776–779, doi: 10.23919/EuCAP.2017.7928095.
[11] B. Yang, Z. Yu, Y. Dong, J. Zhou, and W. Hong, "Compact tapered slot antenna array for 5G millimeter-wave massive MIMO systems," *IEEE Trans. Antennas Propag.*, vol. 65, no. 12, pp. 6721–6727, Dec. 2017, doi: 10.1109/TAP.2017.2700891.
[12] Y. Cheon and Y. Kim, "Millimeter-wave phased array antenna with wide beam coverage," in *Proc. 10th Eur. Conf. Antennas Propag. (EuCAP)*, Davos, Switzerland, Apr. 2016, pp. 1–3, doi: 10.1109/EuCAP.2016.7481337.
[13] S.-M. Moon, S. Yun, I.-B. Yom, and H. L. Lee, "Phased array shaped-beam satellite antenna with boosted-beam control," *IEEE Trans. Antennas Propag.*, vol. 67, no. 12, pp. 7633–7636, Dec. 2019, doi: 10.1109/TAP.2019.2930129.
[14] M. M. M. Ali and A.-R. Sebak, "Design of compact millimeter wave massive MIMO dual-band (28/38 GHz) antenna array for future 5G communication systems," in *Proc. 17th Int. Symp. Antenna Technol. Appl. Electromagn. (ANTEM)*, Montreal, QC, Canada, Jul. 2016, pp. 1–2, doi: 10.1109/ANTEM.2016.7550213.
[15] A. V. Raisanen, J. Zheng, J. Ala-Laurinaho, S. Karki, and V. Viikari, "Millimeter-wave antennas for 5G," in *Proc. 11th Global Symp. Millim. Waves (GSMM)*, Boulder, CO, USA, 2018, pp. 1–4, doi: 10.1109/GSMM.2018.8439370.
[16] C. A. Fernandes and L. M. Anunciada, "Constant flux illumination of square cells for mm-wave wireless communications," in *Proc. Asia–Pacific Microw. Conf.*, Sydney, NSW, Australia, 2000, pp. 1580–1583, doi: 10.1109/APMC.2000.926142.
[17] D. Nyzovets and Y. Yashchyshyn, "A mm-wave beam-steerable leaky-wave antenna with ferroelectric substructure," in *Proc. 13th Eur. Conf. Antennas Propag. (EuCAP)*, Kraków, Poland, 2019, pp. 1–3.
[18] S. K. Koul and G. S. Karthikeya, *Millimeter Wave Antennas for 5G Mobile Terminals and Base Stations*, 1st ed. Boca Raton, FL, USA: CRC Press, 2020, doi: 10.1201/9781003010265.
[19] M. Beccaria, A. Massaccesi, P. Pirinoli, and L. H. Manh, "Multibeam transmitarrays for 5G antenna systems," in *Proc. IEEE 7th Int. Conf. Commun. Electron. (ICCE)*, Hue, Vietnam, Jul. 2018, pp. 217–221, doi: 10.1109/CCE.2018.8465715.
[20] H. Nematollahi, J.-J. Laurin, M. Barba, and J. A. Encinar, "Realization of focused beam and shaped beam transmitarrays based on broadband unit cells," *IEEE Trans. Antennas Propag.*, vol. 65, no. 8, pp. 4368–4373, Aug. 2017, doi: 10.1109/TAP.2017.2717969.
[21] J. Tao, X. Li, Y. Li, F. Teng, and H. Wu, "SIW-fed double layer end-fire metasurface antenna array with improved gain," in *Proc. Cross Strait Quad-Regional Radio Sci. Wireless Technol. Conf. (CSQRWC)*, Taiyuan, China, Jul. 2019, pp. 1–3, doi: 10.1109/CSQRWC.2019.8799107.
[22] Z. Mousavirazi, M. B. Kakhki, T. A. Denidni, and V. Rafii, "MM-wave beam-steering slot antenna using gradient relative-permittivity FSS superstrate," in *Proc. IEEE Int. Symp. Antennas Propag. USNC-URSI Radio Sci. Meeting*, Atlanta, GA, USA, Jul. 2019, pp. 319–320, doi: 10.1109/APUSNCURSINRSM.2019.8888515.
[23] G. Minatti, S. Maci, P. De Vita, A. Freni, and M. Sabbadini, "A metasurface antenna for space application," in *Proc. Int. Symp. Antennas Propag. (ISAP)*, 2012, pp. 870–873.
[24] P. Naseri, S. A. Matos, J. R. Costa, and C. A. Fernandes, "Phase-delay versus phase-rotation cells for circular polarization transmit arrays—Application to satellite Ka-band beam steering," *IEEE Trans. Antennas Propag.*, vol. 66, no. 3, pp. 1236–1247, Mar. 2018, doi: 10.1109/TAP.2017.2787540.
[25] J. Huang and J. A. Encinar, *Reflectarray Antennas*. Hoboken, NJ, USA: Wiley, 2008.
[26] M. H. Dahri, M. I. Abbasi, M. H. Jamaluddin, and M. R. Kamarudin, "A review of high gain and high efficiency reflectarrays for 5G communications," *IEEE Access*, vol. 6, pp. 5973–5985, 2017, doi: 10.1109/ACCESS.2017.2786862.
[27] S. Kausar, S. Shad, A. Kausar, and H. Mehrpouyan, "Design of high gain low cost beam-steering reflectarray antenna," in *Proc. IEEE Int. Symp. Antennas Propag. USNC, URSI Radio Sci. Meeting*, Atlanta, GA, USA, Jul. 2019, pp. 315–316, doi: 10.1109/APUSNCURSINRSM.2019.8888928.
[28] P. Nayeri, F. Yang, and A. Z. Elsherbeni, "Design and experiment of a single-feed quad-beam reflectarray antenna," *IEEE Trans. Antennas Propag.*, vol. 60, no. 2, pp. 1166–1171, Feb. 2012, doi: 10.1109/TAP.2011.2173126.
[29] M. Arrebola, J. A. Encinar, and M. Barba, "Multifed printed reflectarray with three simultaneous shaped beams for LMDS central station antenna," *IEEE Trans. Antennas Propag.*, vol. 56, no. 6, pp. 1518–1527, Jun. 2008, doi: 10.1109/TAP.2008.923360.
[30] A. F. Vaquero, M. Arrebola, M. R. Pino, R. Florencio, and J. A. Encinar, "Demonstration of a reflectarray with near-field amplitude and phase constraints as compact antenna test range probe for 5G new radio devices," *IEEE Trans. Antennas Propag.*, vol. 69, no. 5, pp. 2715–2726, May 2021, doi: 10.1109/TAP.2020.3030969.
[31] D. M. Pozar, "Bandwidth of reflectarrays," *Electron. Lett.*, vol. 39, no. 21, pp. 1490–1491, Oct. 2003.
[32] D. R. Prado, M. Arrebola, M. R. Pino, and F. Las-Heras, "Improved reflectarray phase-only synthesis using the generalized intersection approach with dielectric frame and first principle of equivalence," *Int. J. Antennas Propag.*, vol. 2017, pp. 1–11, May 2017, doi: 10.1155/2017/3829390.
[33] O. M. Bucci, G. Franceschetti, G. Mazzarella, and G. Panariello, "Intersection approach to array pattern synthesis," *IEE Proc.-H Microw., Antennas Propag.*, vol. 137, no. 6, pp. 349–357, Dec. 1990.
[34] O. Bucci, G. D'Elia, G. Mazzarella, and G. Panariello, "Antenna pattern synthesis: A new general approach," *Proc. IEEE*, vol. 82, no. 3, pp. 358–371, Mar. 1994.
[35] C. Wan and J. A. Encinar, "Efficient computation of generalized scattering matrix for analyzing multilayered periodic structures," *IEEE Trans. Antennas Propag.*, vol. 43, no. 11, pp. 1233–1242, Nov. 1995, doi: 10.1109/8.475095.
[36] L. Mohjazi, M. Al-Qutayri, H. Barada, K. Poon, and R. Shubair, "Deployment challenges of femtocells in future indoor wireless networks," presented at the IEEE GCC Conf. Exhib., Feb. 2011, doi: 10.1109/IEEEGCC.2011.5752539.
[37] R. J. Weiter, M. Peter, W. Keusgen, E. Calvanese-Strinati, A. De Domenico, I. Filippini, A. Capone, I. Siaud, A.-M. Ulmer-Moll, A. Maltsev, T. Haustein, and K. Sakaguchi, "Enabling 5G backhaul and access with millimeter-waves," presented at the Eur. Conf. Netw. Commun. (EuCNC), Aug. 2014, pp. 1–5, doi: 10.1109/EuCNC.2014.6882644.
[38] D. R. Prado, J. Álvarez, M. Arrebola, M. R. Pino, R. G. Ayestarán, and F. Las-Heras, "Efficient, accurate and scalable reflectarray phase-only synthesis based on the Levenberg–Marquardt algorithm," *Appl. Comput. Electromagn. Soc. J.*, vol. 30, no. 12, pp. 1246–1255, Dec. 2015.
[39] D. R. Prado, J. A. L. Fernández, M. Arrebola, M. R. Pino, and G. Goussetis, "General framework for the efficient optimization of reflectarray antennas for contoured beam space applications," *IEEE Access*, vol. 6, pp. 72295–72310, 2018.
[40] *Dassault Systems: CST Studio Suite*. Accessed: Jan. 25, 2022. [Online]. Available: https://www.3ds.com/es/productos-y-servicios/simulia/productos/cst-studio-suite/
[41] *TICRA: GRASP | Reflector Antenna Design Software*. Accessed: Jan. 25, 2022. [Online]. Available: https://www.ticra.com/software/grasp/
[42] *TICRA: SNIFT | Spherical Near-Field to Far-Field Transformation*. Accessed: Jan. 25, 2022. [Online]. Available: https://www.ticra.com/software/snift/
[43] H.-T. Chou, T.-M. Hung, N.-N. Wang, H.-H. Chou, C. Tung, and P. Nepa, "Design of a near-field focused reflectarray antenna for 2.4 GHz RFID reader applications," *IEEE Trans. Antennas Propag.*, vol. 59, no. 3, pp. 1013–1018, Mar. 2011.

[44] F. Zhao and Y. J. Cheng, "Near-field focused reflectarray antenna at 140 GHz," in *IEEE MTT-S Int. Microw. Symp. Dig.*, May 2018, pp. 1–4.
[45] S. Yu and L. Li, "Design of near-field focused power-combining reflectarray," in *Proc. 10th Eur. Conf. Antennas Propag. (EuCAP)*, Apr. 2016, pp. 1–2.
[46] G. Carluccio, A. Mazzinghi, and A. Freni, "Design and manufacture of cosecant-squared complementary reflectarrays for low-cost applications," *IEEE Trans. Antennas Propag.*, vol. 65, no. 10, pp. 5220–5227, Oct. 2017, doi: 10.1109/TAP.2017.2743743.
[47] R. R. Elsharkawy, M. Hindy, A. A. Saleeb, and E.-S.-M. El-Rabaie, "A reflectarray with octagonal unit cells for 5-G applications," *Wireless Pers. Commun.*, vol. 97, no. 2, pp. 2999–3016, Nov. 2017, doi: 10.1007/s11277-017-4657-6.

BORJA IMAZ-LUEJE (Student Member, IEEE) was born in Riaño, Asturias, Spain, in 1995. He received the B.Sc. and M.Sc. degrees in telecommunications engineering from the Universidad de Oviedo at Gijón, Spain, in 2017 and 2019, respectively, where he is currently pursuing the Ph.D. degree.

Since 2016, he has been a Research Assistant with the Signal Theory and Communications Area, Universidad de Oviedo. From 2018 to 2019, he spent several months in a fellowship with Rohde & Schwarz GmbH & Company KG, Munich, Germany, where he was involved in the deployment of CATR systems and OTA measurements. His current research interests include the development of efficient analysis and design techniques of reflectarrays in complex configurations, working in environments of near- and far-field.

ÁLVARO F. VAQUERO (Graduate Student Member, IEEE) was born in Salinas, Spain, in 1990. He received the B.Sc., M.Sc., and Ph.D. degrees in telecommunications engineering from the Universidad de Oviedo, Gijón, Spain, in 2015, 2017, and 2021, respectively.

From 2016 to 2021, he was a Research Assistant with the Signal Theory and Communications Area, University of Oviedo. In 2017, he was with the Antennas and Propagation Group, Instituto de Telecomunicações, Lisbon, Portugal, where he was involved in the development of broadband planar lenses for imaging applications. In 2021, he collaborated as a Visiting Scholar with the Antennas and Propagation Group, in the design of beam scanning transmitarray antennas. In December 2021, he joined the Group of Applied Electromagnetics, Department of Signals, Systems, and Radiocommunications, Universidad Politécnica de Madrid, Madrid, where he is currently a Postdoctoral Researcher working in the synthesis of reflective intelligent surfaces (RIS) for 5G/B5G networks. His current research interests include the development of efficient techniques for the analysis and synthesis of planar antennas, especially reflectarray, transmitarray and reconfigurable intelligent surfaces (RIS) for near-field applications, and the design of additive manufacturing antennas in mm-wave frequencies.

DANIEL R. PRADO was born in Sama de Langreo, Asturias, Spain, in 1986. He received the B.Sc., M.Sc., and Ph.D. degrees in telecommunication engineering from the University of Oviedo, Gijón, Spain, in 2011, 2012, and 2016, respectively.

From 2010 to 2011, he was with the Institute of Electronics, Communications and Information Technology, Queen's University Belfast, Belfast, U.K., where he was involved in the design of leaky-wave antennas as part of his B.Sc. research project. From 2011 to 2017, he was a Research Assistant with the Signal Theory and Communications Area, University of Oviedo, where he was involved in the development of efficient techniques for the analysis and synthesis of reflectarray antennas. In 2014, he was with the School of Electrical Engineering, KTH Royal Institute of Technology, Stockholm, Sweden, as a Visiting Scholar, where he was involved in transformation optics applied to dielectric lenses. From 2018 to 2019, he was with the Institute of Sensors, Signals and Systems, Heriot-Watt University, Edinburgh, U.K. Since 2020, he has been with the Signal Theory and Communications Area, University of Oviedo, as a Postdoctoral Researcher. His current research interests include the analysis of nonuniform arrays and the development of efficient techniques for the analysis and optimization of near and far fields of reflectarray antennas.

Dr. Prado was a recipient of a Predoctoral Scholarship financed by the Gobierno del Principado de Asturias, a Postdoctoral Fellowship partially financed by the European Union, and a Postdoctoral Fellowship financed by the Spanish Government.

MARCOS R. PINO was born in Vigo, Spain, in 1972. He received the M.Sc. and Ph.D. degrees in telecommunication engineering from the University of Vigo, Spain, in 1997 and 2000, respectively.

In 1998, he was a Visiting Scholar with the ElectroScience Laboratory, The Ohio State University, Columbus, OH, USA. From 2000 to 2001, he was an Assistant Professor with the University of Vigo. Since 2001, he has been with the Electrical Engineering Department, University of Oviedo at Gijón, Spain, where he is currently a Full Professor, teaching courses on communication systems and antenna design. From 2017 to 2019, he has spent several months as a Visiting Fellow with the Department of Information Engineering, University of Pisa, Italy, collaborating in near-field UHF-RFID applications. His current research interests include antenna design optimized for both near-field and far-field applications, antenna measurement techniques, and efficient computational techniques applied to EM problems.

MANUEL ARREBOLA (Senior Member, IEEE) was born in Lucena, Córdoba, Spain. He received the M.Sc. degree in telecommunication engineering from the University of Málaga, Málaga, Spain, in 2002, and the Ph.D. degree from the Technical University of Madrid (UPM), Madrid, Spain, in 2008.

From 2003 to 2007, he was a Research Assistant with the Department of Electromagnetism and Circuit Theory, UPM. In 2005, he was a Visiting Scholar with the Department of Microwave Techniques, Universität Ulm, Ulm, Germany. In 2007, he joined the Department of Electrical Engineering, University of Oviedo at Gijón, Spain, where he is currently an Associate Professor. In 2009, he was with the European Space Research and Technology Centre, European Space Agency, Noordwijk, The Netherlands, for a period of two months. In 2018, he was a Visiting Professor with the Edward S. Rogers Sr. Department of Electrical and Computer Engineering, University of Toronto, Toronto, ON, Canada. In 2019, he was a Visiting Professor with the Institute of Sensors, Signals and Systems, Heriot-Watt University, Edinburgh, U.K. His current research interests include the development of efficient analysis, design, and optimization techniques of reflectarray and transtmitarray antennas both in near- and far-fields.

Dr. Arrebola was a co-recipient of the 2007 S. A. Schelkunoff Transactions Prize Paper Award by the IEEE Antennas and Propagation Society.